Journal of Molecular Cell Biology (2024), 16(11), mjae056 https://doi.org/10.1093/jmcb/mjae056
Published online December 23, 2024

Article

DNAJC12 downregulation induces neuroblastoma progression via increased histone H4K5 lactylation

Yaqi Yang[1,†], Jiejun Wen[1,†], Susu Lou[1,2,†], Yali Han[3], Yi Pan[1], Ying Zhong[1], Qiao He[4], Yinfeng Zhang[1], Xi Mo[1,*], Jing Ma[4,*], and Nan Shen[1,5,*]

[1] Pediatric Translational Medicine Institute, Shanghai Children's Medical Center, Shanghai Jiao Tong University School of Medicine, Shanghai 200127, China
[2] Pediatric Department, The Affiliated Hospital of Hangzhou Normal University, Hangzhou 310000, China
[3] Department of Hematology and Oncology, Shanghai Children's Medical Center, Shanghai Jiao Tong University School of Medicine, Shanghai 200127, China
[4] Department of Pathology, Shanghai Children's Medical Center, Shanghai Jiao Tong University School of Medicine, Shanghai 200127, China
[5] Department of Infectious Diseases, Shanghai Children's Medical Center, Shanghai Jiao Tong University School of Medicine, Shanghai 200127, China
[†] These authors contributed equally to this work.
* Correspondence to: Nan Shen, E-mail: shennan@scmc.com.cn; Jing Ma, E-mail: majing@scmc.com.cn; Xi Mo, E-mail: xi.mo@shsmu.edu.cn

Edited by Hua Lu

Neuroblastoma (NB) is the most common extracranial solid tumor in children. Despite treatment advances, the survival rates of high-risk NB patients remain low. This highlights the urgent need for a deeper understanding of the molecular mechanisms driving NB progression to support the development of new therapeutic strategies. In this study, we demonstrated that the reduced levels of DNAJC12, a protein involved in metabolic regulation, are associated with poor prognosis in NB patients. Our data indicate that low DNAJC12 expression activates glycolysis in NB cells, leading to increased lactic acid production and histone H4 lysine 5 lactylation (H4K5la). Elevated H4K5la upregulates the transcription of *COL1A1*, a gene implicated in cell metastasis. Immunohistochemistry staining of NB patient samples confirmed that high H4K5la levels correlate with poor clinical outcomes. Furthermore, we showed that inhibiting glycolysis, reducing H4K5la, or targeting *COL1A1* can mitigate the invasive behavior of NB cells. These findings reveal a critical link between metabolic reprogramming and epigenetic modifications in the context of NB progression, suggesting that H4K5la could serve as a novel diagnostic and prognostic marker, and shed light on identifying new therapeutic targets within metabolic pathways for the treatment of this aggressive pediatric cancer.

Keywords: histone H4K5 lactylation, DNAJC12, COL1A1, neuroblastoma, biomechanical force

Introduction

Neuroblastoma (NB), the most prevalent extracranial solid tumor in pediatric patients, is a formidable challenge in pediatric oncology and is characterized by heterogenous outcomes and high mortality rates (Verhoeven et al., 2022; Friedman et al., 2024). Despite advancements in multimodal anticancer treatments, including surgery, chemotherapy, radiation, and GD2 mAb-based immunotherapy, the survival rates of children diagnosed with high-risk NB have shown limited improvement (Ladenstein et al., 2018; Yu et al., 2021; Spencer et al., 2022). This underscores the urgent need for innovative therapeutic targets and prognostic markers.

Within the realm of molecular oncology, members of the DNAJ heat shock protein family (HSP40) have emerged as promising targets. This family, comprising >40 evolutionarily conserved members, orchestrates critical cellular processes such as protein folding and transcriptional regulation (Gu et al., 2020; Liu et al., 2020). The differential expression of these proteins across tissues has been linked to either the promotion or inhibition of cancer progression, identifying specific DNAJ proteins as crucial prognostic indicators or potential therapeutic targets in cancer research (Sterrenberg et al., 2011; Wu et al., 2017). For example, reduced DNAJB6 levels have been observed in esophageal squamous cell carcinoma (Yu et al., 2015), and DNAJB4 has been

Received June 27, 2024. Revised December 9, 2024. Accepted December 22, 2024.

proposed as a potential biomarker for breast cancer (Acun et al., 2017; Uretmen Kagiali et al., 2019).

DNAJC12, a member of the HSP40 family, functions primarily as a cochaperone involved in the metabolism of aromatic amino acids, which are precursors for catecholamine synthesis (Jung-Kc et al., 2019). Notably, DNAJC12 is highly expressed in the adrenal gland (https://www.proteinatlas.org/) and has been implicated in the migration and invasion dynamics of various cancers (Li et al., 2021; Deng et al., 2024; Shen et al., 2024). Given that NB originates from neural crest cells and often exhibits adrenal-like characteristics, such as the production of catecholamine (Jansky et al., 2021; Ponzoni et al., 2022), it has been hypothesized that DNAJC12 plays a role in NB progression. However, the specific function of DNAJC12 in NB remains unexplored.

In this study, we attempted to address this knowledge gap by exploring the role of DNAJC12 in NB, with a focus on understanding how it can affect tumor progression through mechanisms beyond its established function in catecholamine biosynthesis. By examining the regulatory effects of DNAJC12 on metabolic and epigenetic pathways in NB, we aimed to enhance the molecular underpinnings of NB and identify new therapeutic strategies for this challenging pediatric cancer.

Results

Low DNAJC12 expression promotes NB cell proliferation and invasion

To investigate the role of DNAJC12 in NB, we analyzed its mRNA levels in relation to patient prognosis by using data from 249 NB cases in the Therapeutically Applicable Research to Generate Effective Treatments (TARGET) database (Supplementary Table S1). Kaplan–Meier survival analysis revealed a significant association between *DNAJC12* expression levels and patient outcomes, with lower levels of *DNAJC12* correlating with a shorter median survival of 3.5 years, compared to 7.2 years in patients with higher *DNAJC12* levels (Figure 1A).

To further elucidate the impact of DNAJC12 on NB progression, we generated two DNAJC12 knockout SH-SY5Y cell lines (KO1 and KO2) using clustered regularly interspaced short palindromic repeats (CRISPR)/CRISPR-associated protein 9 (Cas9) gene-editing technology (Figure 1B). BrdU incorporation assays indicated that DNAJC12 knockout significantly increased cell proliferation, and this effect was partially reversed by transient transfection of a DNAJC12-expressing plasmid (Figure 1C). Similarly, Transwell invasion assays revealed that DNAJC12 knockout increased cell invasion ability, which was mitigated by DNAJC12 complementation (Figure 1D). As expected, overexpression of DNAJC12 in SH-SY5Y cells led to significant reductions in both cell proliferation and invasion (Supplementary Figure S1). Consistent results were obtained in another NB cell line, SK-N-SH (Supplementary Figure S2A–C).

Given that metastasis is the primary cause of poor prognosis in NB (Matthay et al., 2016), we focused on the role of DNAJC12 in regulating cell invasion. Gene ontology (GO) and gene set enrichment analysis (GSEA) revealed that the genes significantly upregulated in DNAJC12 KO SH-SY5Y cells were associated with invasion-related pathways, including extracellular matrix (ECM) receptor interaction and focal adhesion (Figure 2A–C; Supplementary Table S2). F-actin (phalloidin) staining revealed increased stress fiber abundance and lamellipodium formation in DNAJC12 KO cells (Figure 2D; Supplementary Figure S2D). Consistently, immunoblotting and quantitative polymerase chain reaction (qPCR) analyses revealed the upregulation of β-catenin, Filamin A, and several integrins, which are key biomarkers for cytoskeleton organization and focal adhesion, in DNAJC12 KO cells (Figure 2E–G). These findings suggest that low DNAJC12 expression may contribute to poor prognosis in NB patients by promoting tumor cell metastasis, potentially through the modulation of signaling pathways related to biomechanical forces.

Low DNAJC12 expression enhances NB cell invasion via glycolysis activation

Considering the involvement of DNAJC12 in metabolic processes, we performed nontargeted mass spectrometry (MS)-based metabolomic analyses on wild-type and DNAJC12 KO SH-SY5Y cells. While intracellular dopamine was undetectable, likely due to its low concentration, we observed significantly increased levels of glycolytic metabolites, including pyruvate and lactic acid, in DNAJC12 KO cells (Figure 3A and B). An L-lactic acid colorimetric assay confirmed the elevated lactic acid levels in DNAJC12 KO cells (Figure 3C). Furthermore, GSEA of RNA sequencing (RNA-seq) data revealed activation of the glycolysis pathway in DNAJC12 KO cells, as evidenced by the upregulated expression of key glycolytic enzymes (Figure 3D and E).

To examine whether the activation of glycolysis is responsible for the enhanced invasion observed in DNAJC12 KO cells, we treated the cells with GNE-140, an inhibitor of lactate dehydrogenase A (LDHA). As expected, treatment with GNE-140 significantly reduced intracellular lactic acid levels (Figure 3F), stress fiber formation (Figure 3G), and the invasion (Figure 3H) of DNAJC12 KO cells without affecting cell viability. Collectively, these findings indicate that DNAJC12 deficiency facilitates NB cell invasion primarily through the activation of glycolysis, which in turn affects cytoskeletal dynamics.

Low DNAJC12 expression enhances NB cell invasion via histone lactylation

Although the activation of glycolysis is a hallmark of tumor cells (the 'Warburg Effect'), the precise role of lactic acid in tumor progression remains incompletely understood. Recent studies have suggested that lactic acid can covalently modify lysine residues in histones, resulting in histone lactylation (Zhang et al., 2019). On the basis of these findings, we hypothesized that DNAJC12 knockout might enhance cell invasion through increasing histone lactylation. Immunoblotting analysis revealed a significant increase in pan-lactylation levels in DNAJC12 KO cells (Figure 4A). We further assessed specific histone lactylation sites using commercially available antibodies suitable for chromatin immunoprecipitation followed by sequencing

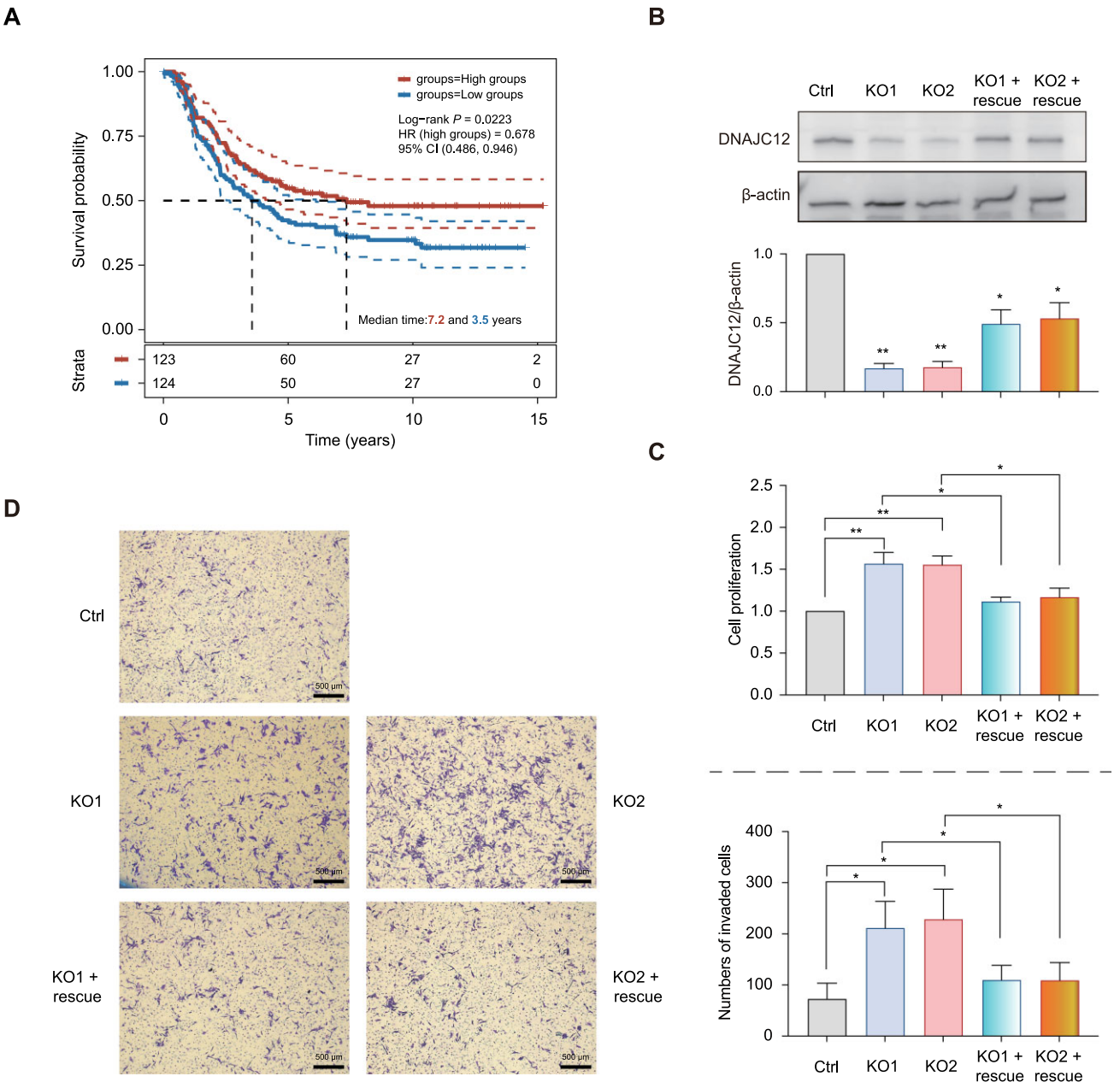

Figure 1 Low DNAJC12 expression promotes NB cell proliferation and invasion, correlating with poor prognosis in NB patients. (**A**) Kaplan–Meier survival analysis of 279 NB patients from the TARGET database, stratified by *DNAJC12* expression levels. Survival differences between high- and low-expression groups were analyzed using the log-rank test. (**B**) DNAJC12 KO SH-SY5Y cells were generated using CRISPR/Cas9, with complementation of DNAJC12 achieved via lentiviral transfection. DNAJC12 protein levels were assessed by immunoblotting, and the relative band intensity was quantified using ImageJ, normalized to that of β-actin, and expressed as the fold change relative to control (wild-type) cells. (**C**) Cell proliferation rates of DNAJC12 KO and complemented SH-SY5Y cells were measured via BrdU chemiluminescent assays and compared with those of control cells. (**D**) Cell invasion was assessed in DNAJC12 KO and complemented SH-SY5Y cells via Transwell assays, and the number of invaded cells was quantified. Scale bar, 10 μm. The data are presented as mean ± SEM from three independent experiments. Statistical significance was determined via two-tailed Student's *t*-test (*$P < 0.05$; **$P < 0.01$).

(ChIP–seq) assays. Among the eight histone lactylation sites detected, four (H4K5la, H2BK16la, H3K9la, and H4K8la) exhibited a significant increase in lactylation upon DNAJC12 knockout (Figure 4B; Supplementary Figures S2E and S3). These results suggest that DNAJC12 knockout indeed enhances histone lactylation, potentially contributing to increased NB cell invasion.

To evaluate the relevance of histone lactylation for patient prognosis, we performed immunohistochemistry (IHC)

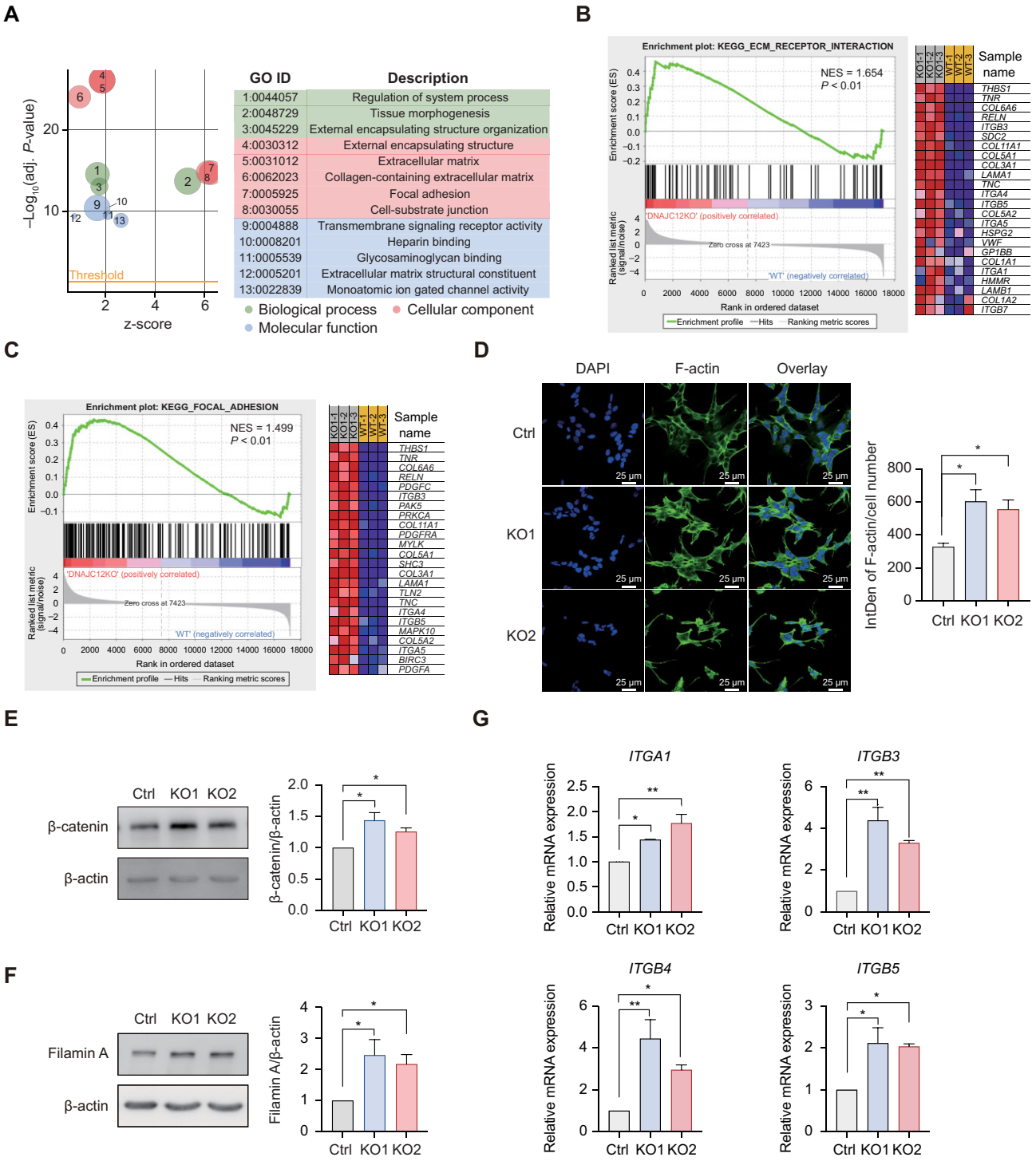

Figure 2 Low DNAJC12 expression enhances NB cell invasion by activating signaling related to biomechanical force. (**A**) GO analysis for pathways enriched in DNAJC12 KO1 SH-SY5Y cells. (**B** and **C**) GSEA of genes related to ECM receptor interaction (**B**) and focal adhesion (**C**) was performed on 3 independent RNA-seq datasets from control and DNAJC12 KO1 SH-SY5Y cells. (**D**) Immunofluorescence staining showing a significant increase in F-actin levels in DNAJC12 KO SH-SY5Y cells. The average fluorescence intensity per cell was quantified using ImageJ. Scale bar, 25 μm. (**E** and **F**) The protein levels of β-catenin and Filamin A, normalized to β-actin. (**G**) The mRNA levels of integrins involved in ECM receptor interaction and focal adhesion in control and DNAJC12 KO SH-SY5Y cells were quantified by qPCR. The data are presented as mean ± SEM from three independent experiments. Statistical significance was determined via two-tailed Student's *t*-test (*$P < 0.05$; **$P < 0.01$).

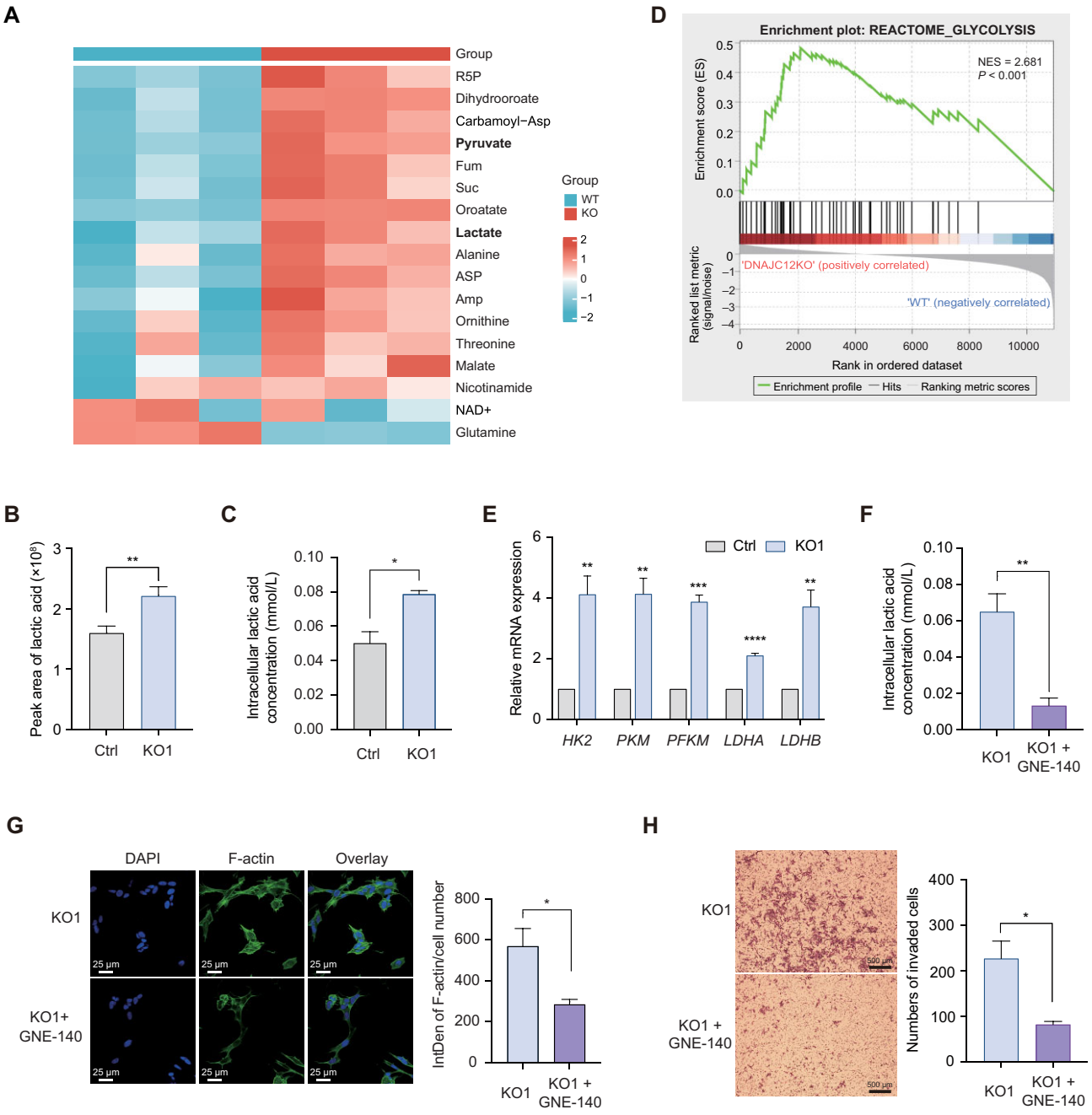

Figure 3 Low DNAJC12 expression enhances NB cell invasion and signaling related to biomechanical force through the activation of glycolysis. (**A**) Heatmap showing the metabolomic profiles of control and DNAJC12 KO1 SH-SY5Y cells, highlighting 17 metabolites with significantly altered abundance. (**B**) Lactic acid levels in control and DNAJC12 KO1 SH-SY5Y cells were measured via MS-based metabolomics. (**C**) Intracellular lactic acid concentrations were quantified via an L-lactic acid colorimetric assay. (**D**) GSEA of glycolysis-related genes was performed on three independent RNA-seq datasets from control and DNAJC12 KO1 cells. (**E**) The mRNA levels of key glycolytic enzymes (*HK2*, *PKM*, *PFKM*, *LDHA*, and *LDHB*) in control and DNAJC12 KO1 SH-SY5Y cells. (**F**) Intracellular lactic acid concentrations in DNAJC12 KO1 SH-SY5Y cells treated with DMSO or the LDHA inhibitor GNE-140 (10 μM). (**G**) Immunofluorescence staining of F-actin in DNAJC12 KO1 SH-SY5Y cells treated with or without GNE-140 (10 μM). Scale bar, 25 μm. (**H**) The invasion ability of DNAJC12 KO1 SH-SY5Y cells treated with or without GNE-140. Scale bar, 10 μm. The data are presented as mean ± SEM from three independent experiments. Statistical significance was determined via two-tailed Student's *t*-test (*$P < 0.05$; **$P < 0.01$; ***$P < 0.001$; ****$P < 0.0001$).

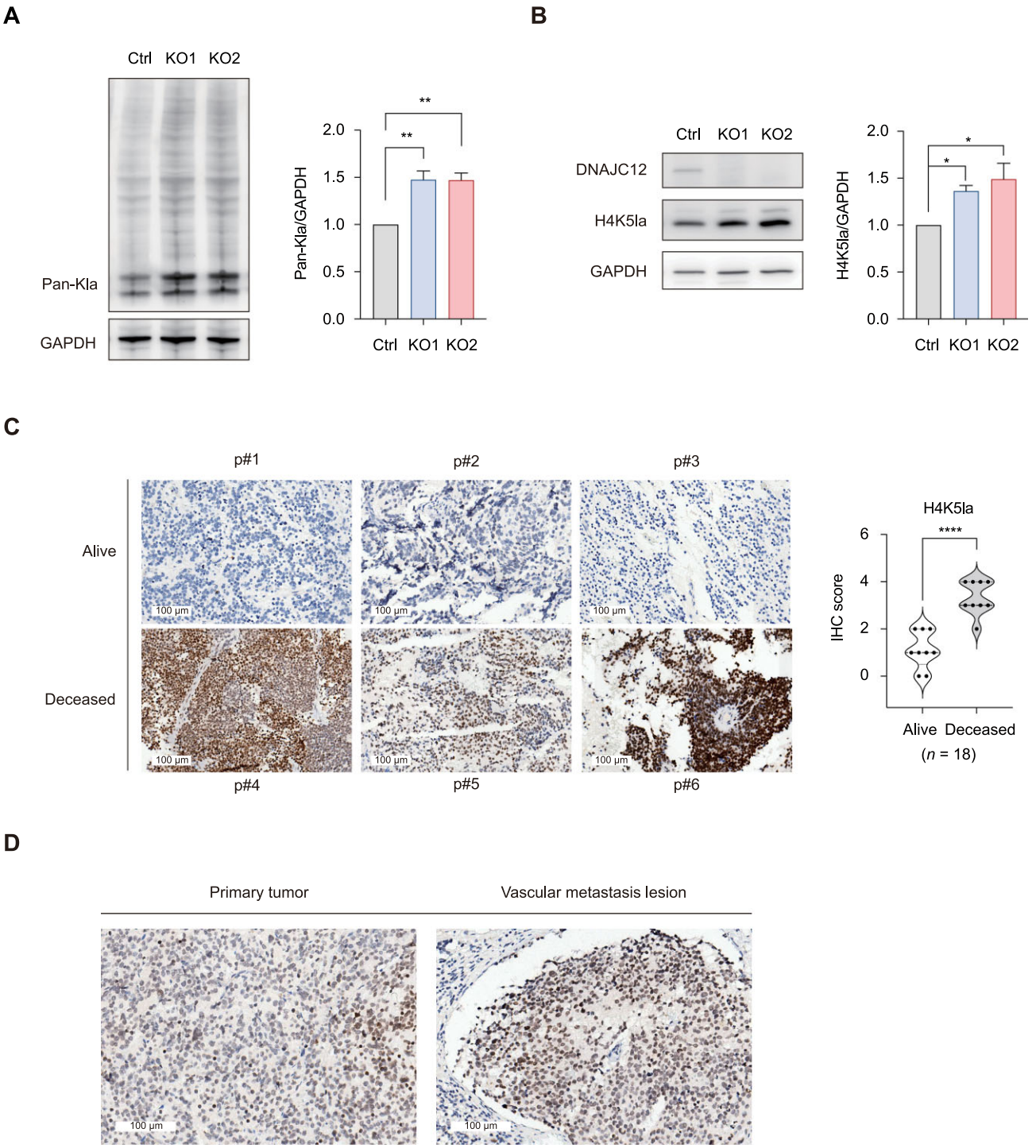

Figure 4 Low DNAJC12 expression enhances NB cell invasion via histone lactylation. (**A**) Pan-lactylation (Pan-Kla) levels in control and DNAJC12 KO SH-SY5Y cells, normalized to GAPDH. (**B**) H4K5la modification levels in control and DNAJC12 KO SH-SY5Y cells. (**C**) IHC staining of H4K5la modification in NB tumor tissues, with IHC scores and patient prognosis ($n = 18$) shown in the right panel. Scale bar, 100 μm. (**D**) IHC staining of H4K5la modification in primary tumor tissues and vascular metastasis tissues. Scale bar, 100 μm. The data are presented as mean ± SEM from three independent experiments. Statistical significance was determined using two-tailed Student's *t*-test (*$P < 0.05$; **$P < 0.01$; ****$P < 0.0001$).

staining on tissue sections from NB patients admitted to our hospital in 2018 and 2019, using antibodies against H4K5la, H2BK16la, H3K9la, and H4K8la. Notably, high levels of H4K5la were significantly associated with poor prognosis in NB patients (Figure 4C; Supplementary Figure S4). Importantly, in one patient sample, the tumor cells that had metastasized into blood vessels exhibited even greater H4K5la levels than primary tumor cells (Figure 4D), suggesting a potential role for H4K5la in tumor metastasis. In contrast, anti-H4K8la antibodies yielded suboptimal IHC staining results, and the levels of H2BK16la and H3K9la did not correlate with patient prognosis (Supplementary Figure S5).

SIRT2 and p300/CBP regulate H4K5la modification in NB cells

Histone modifications, including lactylation, are regulated by specific enzymes known as 'writers' and 'erasers'. Our previous study revealed that SIRT2 functions as a histone delactylase at specific sites in NB cells (Zu et al., 2022). Consistently, we also observed a significant decrease in the H4K5la level of NB cells transiently overexpressing wild-type SIRT2 ($SIRT2^{OE}$), but not a catalytic-activation mutant SIRT2 ($SIRT2^{Q167A}$) (Finnin et al., 2001; Figure 5A), indicating that SIRT2 can serve as the 'eraser' for H4K5la in NB cells. As expected, overexpression of $SIRT2^{OE}$ but not $SIRT2^{Q167A}$ significantly reduced cell proliferation and invasion in DNAJC12 KO cells without affecting intracellular lactic acid levels (Figure 5B–D).

The histone acetyltransferase p300, which was previously reported to mediate lactylation *in vitro* (Zhang et al., 2019), was investigated as a potential 'writer' for H4K5la in NB cells. Treatment with the p300/CBP inhibitor anacardic acid significantly reduced H4K5la levels in DNAJC12 KO cells as well as cell proliferation, stress fiber formation, and invasion, without altering lactic acid levels (Figure 5E–I). These findings suggest that SIRT2 and p300/CBP function as the 'eraser' and 'writer' for H4K5la, respectively, thus regulating the metastatic phenotype of NB cells.

H4K5la promotes NB cell invasion by activating COL1A1 transcription

To identify genes regulated by H4K5la modification, we performed ChIP–seq using an anti-H4K5la antibody in both wild-type and DNAJC12 KO SH-SY5Y cells (Supplementary Tables S3 and S4). This analysis revealed 1937 peaks corresponding to 1277 genes in wild-type cells and 2744 peaks corresponding to 1766 genes in DNAJC12 KO cells (Figure 6A). Notably, 1208 genes were uniquely associated with H4K5la in DNAJC12 KO cells, with the majority of these modifications located in promoter regions (Figure 6B). A significant increase in H4K5la marks at the transcription start site (TSS) was observed upon DNAJC12 knockout (Figure 6C), supporting the role of histone lactylation as a transcription-activating modification (Wang et al., 2022b).

GO analysis revealed that the genes significantly differentially expressed in DNAJC12 KO cells were enriched in pathways related to biomechanical force and metastasis, including cell adhesion molecule binding and actin binding (Figure 6D). To further elucidate the role of H4K5la in regulating biomechanical force and facilitating cell invasion, we cross-referenced our RNA-seq and ChIP–seq datasets to identify genes that were (i) significantly upregulated upon DNAJC12 knockout, (ii) specifically bound by the anti-H4K5la antibody, and (iii) critical for cell migration or invasion. Through this analysis, we identified *COL1A1*, encoding type I collagen protein, which is a key regulator of the ECM (Figure 6E). ChIP–qPCR analysis confirmed significantly greater enrichment of H4K5la at the *COL1A1* locus in DNAJC12 KO cells than in wild-type cells (Figure 6F). Additionally, qPCR analysis demonstrated a substantial increase in *COL1A1* transcription upon DNAJC12 knockout (Figure 6G). These findings suggest that H4K5la modification may promote NB cell invasion by activating *COL1A1* transcription.

To validate the role of *COL1A1* in DNAJC12 KO-induced NB cell invasion, we silenced *COL1A1* expression via small-interfering RNA (siRNA) and treated the cells with the specific inhibitor halofuginone. Both approaches effectively reduced *COL1A1* mRNA and protein levels without affecting cell viability and impaired the invasive capacity of DNAJC12 KO cells (Figure 7; Supplementary Figure S2H–K), confirming that *COL1A1* is a critical downstream effector of DNAJC12 knockout and H4K5la modification.

Discussion

In this study, we identified a novel link between low DNAJC12 levels and poorer outcomes in NB patients. Our findings suggest that this relationship is mediated by the elevated levels of lactic acid and a consequent increase in H4K5la modification. This modification is crucial for transcriptional regulation of the *COL1A1* gene, which plays a significant role in the ECM pathway, affecting cell adhesion and possibly enhancing the metastatic capabilities of NB cells. Our research reveals the complex interplay between metabolic changes and epigenetic modifications in the control of tumor progression and prognosis of NB patients. Furthermore, the emergence of H4K5la as a potential prognostic marker offers insights into NB that could guide the refinement of diagnostic and therapeutic strategies, representing a small but impartment step toward more personalized treatment modalities.

While DNAJC12 is expressed in various tissues, including renal tissues, our study focused on NB due to its distinct neuroendocrine characteristics. NB arises from neural crest cells and frequently displays adrenal-like features, such as catecholamine production, which are crucial for tumor biology and clinical outcomes (Jansky et al., 2021; Ponzoni et al., 2022). Our findings indicate that the role of DNAJC12 in NB is mediated through mechanisms involving glycolysis and epigenetic reprogramming. Interestingly, DNAJC12 appears to have a context-dependent function in cancer metabolism. In addition to its established role in monoamine synthesis (Anikster et al., 2017; Deng et al., 2024; Thony et al., 2024), DNAJC12 seems to downregulate glycolysis in NB, which contrasts with its role in non-small cell lung cancer, where high levels of DNAJC12 promote glycolysis via β-catenin activation (Wang et al., 2022a). The

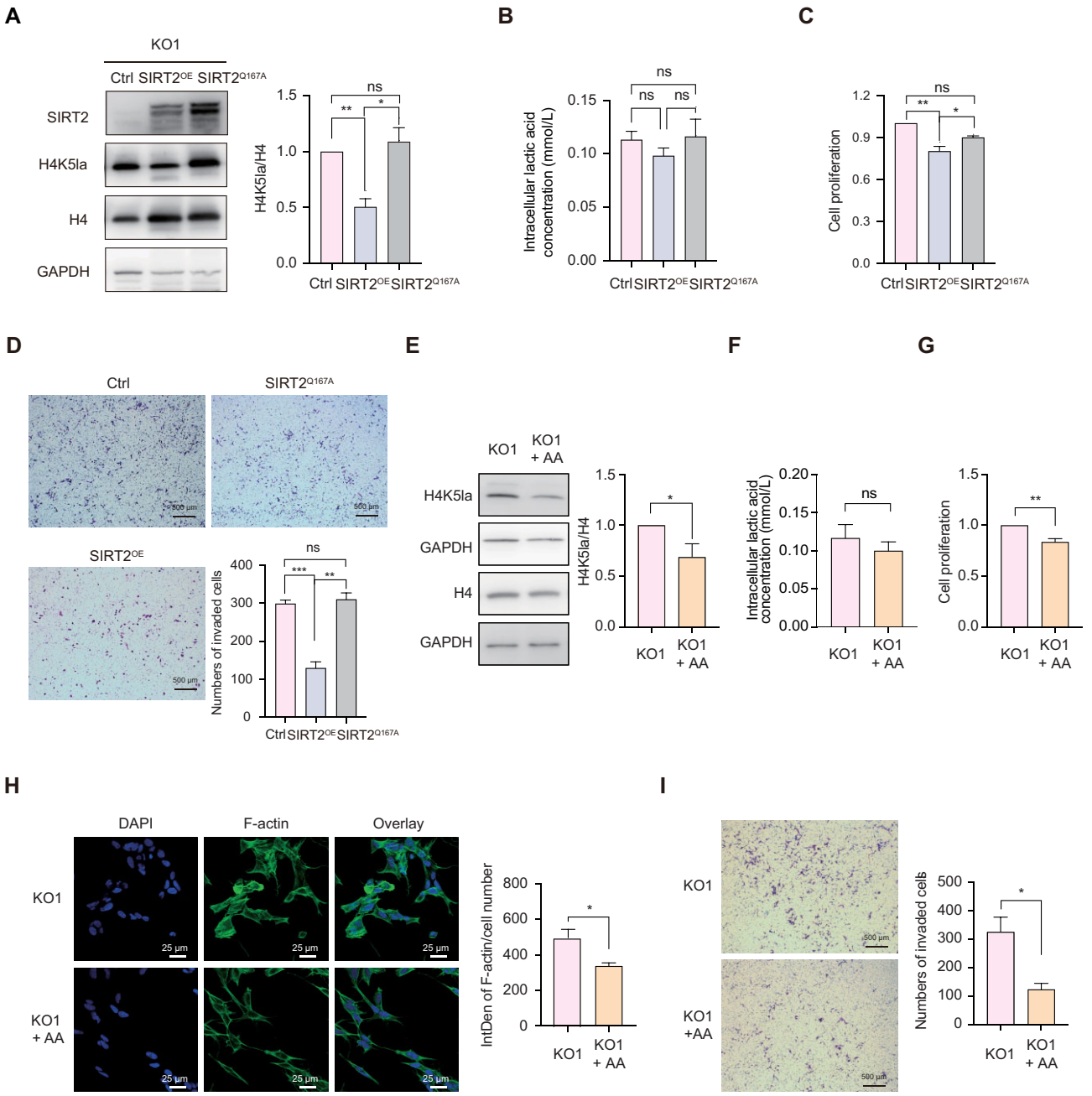

Figure 5 Regulation of H4K5la modification by SIRT2 and p300/CBP in NB cells. (**A**) H4K5la modification levels in DNAJC12 KO1 SH-SY5Y cells with or without transient overexpression of wild-type ($SIRT2^{OE}$) or mutant ($SIRT2^{Q167A}$) SIRT2 plasmids, normalized to H4 and GAPDH. (**B**) Intracellular lactic acid concentrations in DNAJC12 KO1 SH-SY5Y cells with or without transient overexpression of $SIRT2^{OE}$ or $SIRT2^{Q167A}$ plasmids. (**C**) Cell proliferation rates in DNAJC12 KO1 SH-SY5Y cells with or without transient overexpression of $SIRT2^{OE}$ or $SIRT2^{Q167A}$ plasmids. (**D**) The invasion ability of DNAJC12 KO1 SH-SY5Y cells with or without transient overexpression of $SIRT2^{OE}$ or $SIRT2^{Q167A}$ plasmids. Scale bar, 10 μm. (**E**–**I**) DNAJC12 KO1 SH-SY5Y cells were treated with the p300/CBP inhibitor anacardic acid (AA, 10 μM). H4K5la levels (**E**), intracellular lactic acid concentrations (**F**), cell proliferation rates (**G**), F-actin amounts (**H**; scale bar, 25 μm), and cell invasion capability (**I**; scale bar, 10 μm) were measured. The data are presented as mean ± SEM from three independent experiments. Statistical significance was determined using two-tailed Student's *t*-test (*$P < 0.05$; **$P < 0.01$; ns, not significant).

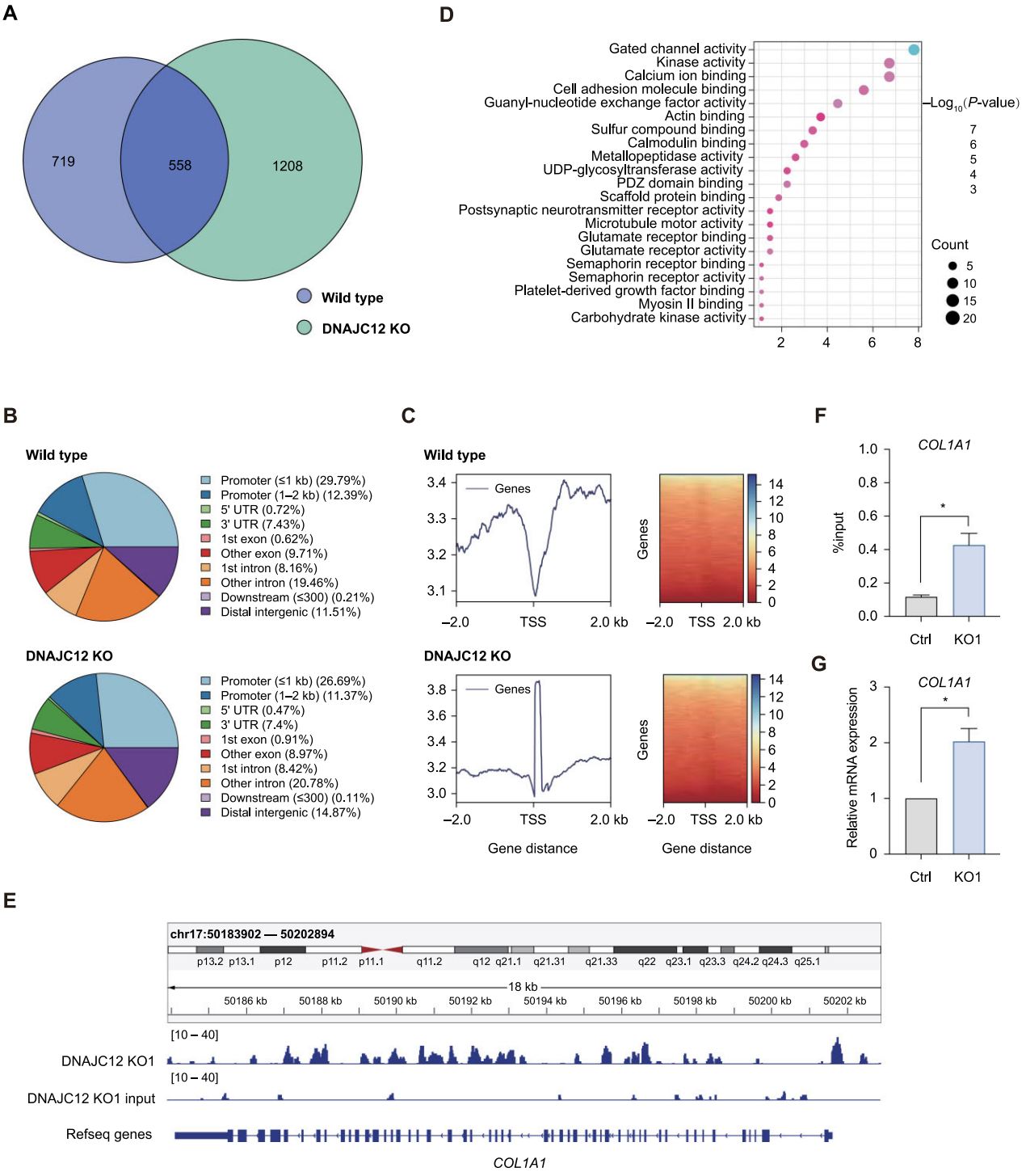

Figure 6 H4K5la modification activates *COL1A1* gene transcription. (**A**) Venn diagram showing genes uniquely identified by the anti-H4K5la antibody in wild-type and DNAJC12 KO1 SH-SY5Y cells. (**B**) Donut chart illustrating the genomic distribution of peaks identified by the anti-H4K5la antibody in wild-type and DNAJC12 KO1 SH-SY5Y cells. Promoters are defined as regions ± 2 kb from the TSS (in the RefSeq database). (**C**) Anchor plot of H4K5la ChIP–seq signals around TSSs in wild-type and DNAJC12 KO1 SH-SY5Y cells. (**D**) GO analysis for the pathways enriched with genes significantly altered expression upon DNAJC12 knockout and were specifically recognized by the anti-H4K5la antibody in DNAJC12 KO1 SH-SY5Y cells. (**E**) Genome browser view of H4K5la signals in the *COL1A1* gene promoter region in DNAJC12 KO1 SH-SY5Y cells. (**F**) ChIP–qPCR analysis of H4K5la occupancy at the *COL1A1* promoter in control and DNAJC12 KO1 SH-SY5Y cells. (**G**) *COL1A1* mRNA levels in control and DNAJC12 KO1 SH-SY5Y cells. The data represent mean ± SEM from three independent experiments. Statistical significance was determined via two-tailed Student's *t*-test (*$P < 0.05$).

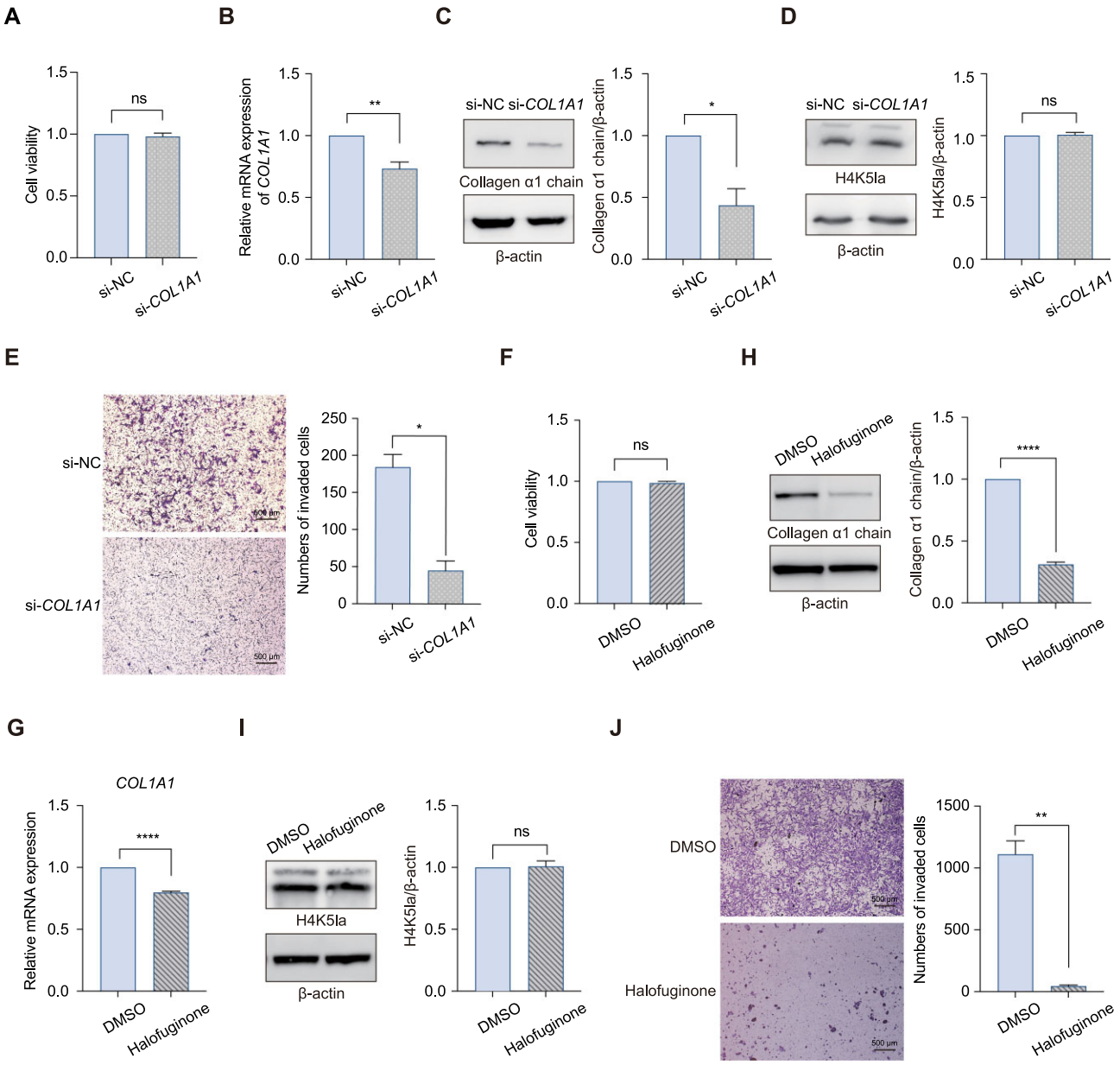

Figure 7 H4K5la modification promotes NB cell invasion by activating *COL1A1* transcription. (**A**) The viability of DNAJC12 KO1 SH-SY5Y cells transfected with or without *COL1A1* siRNA. (**B**) *COL1A1* mRNA levels in DNAJC12 KO1 SH-SY5Y cells transfected with or without *COL1A1* siRNA. (**C** and **D**) Type I collagen α1 chain protein (**C**) and H4K5la (**D**) levels in DNAJC12 KO1 SH-SY5Y cells transfected with or without *COL1A1* siRNA, normalized to β-actin. (**E**) The invasion ability of DNAJC12 KO1 SH-SY5Y cells transfected with or without *COL1A1* siRNA. Scale bar, 10 μm. (**F**) The viability of DNAJC12 KO1 cells treated with DMSO or the type I collagen inhibitor halofuginone (100 nM). (**G**) *COL1A1* mRNA levels in DNAJC12 KO1 cells treated with or without Halofuginone (100 nM). (**H** and **I**) Type I collagen α1 chain protein (**H**) and H4K5la (**I**) levels in DNAJC12 KO1 SH-SY5Y cells treated with or without halofuginone (100 nM), normalized to β-actin. (**J**) Invasion ability of DNAJC12 KO1 SH-SY5Y cells treated with or without halofuginone (100 nM). Scale bar, 10 μm. The data are presented as mean ± SEM from three independent experiments. Statistical significance was determined via two-tailed Student's *t*-test (*$P < 0.05$; **$P < 0.01$; ****$P < 0.0001$; ns, not significant).

underlying mechanisms by which the reduced DNAJC12 levels activate glycolysis in NB cells remain unclear. However, HSPs such as HSP40 can directly interact with pyruvate kinase M2 (PKM2) and destabilize PKM2 through HSC70, leading to the downregulation of glycolysis (Huang et al., 2014). Given the structural similarity of the J domain between DNAJC12 and HSP40, it is plausible that DNAJC12 may inhibit glycolysis via a similar mechanism, a hypothesis that warrants further investigation (Qian et al., 1996). The contrasting effects of DNAJC12 on glycolysis in

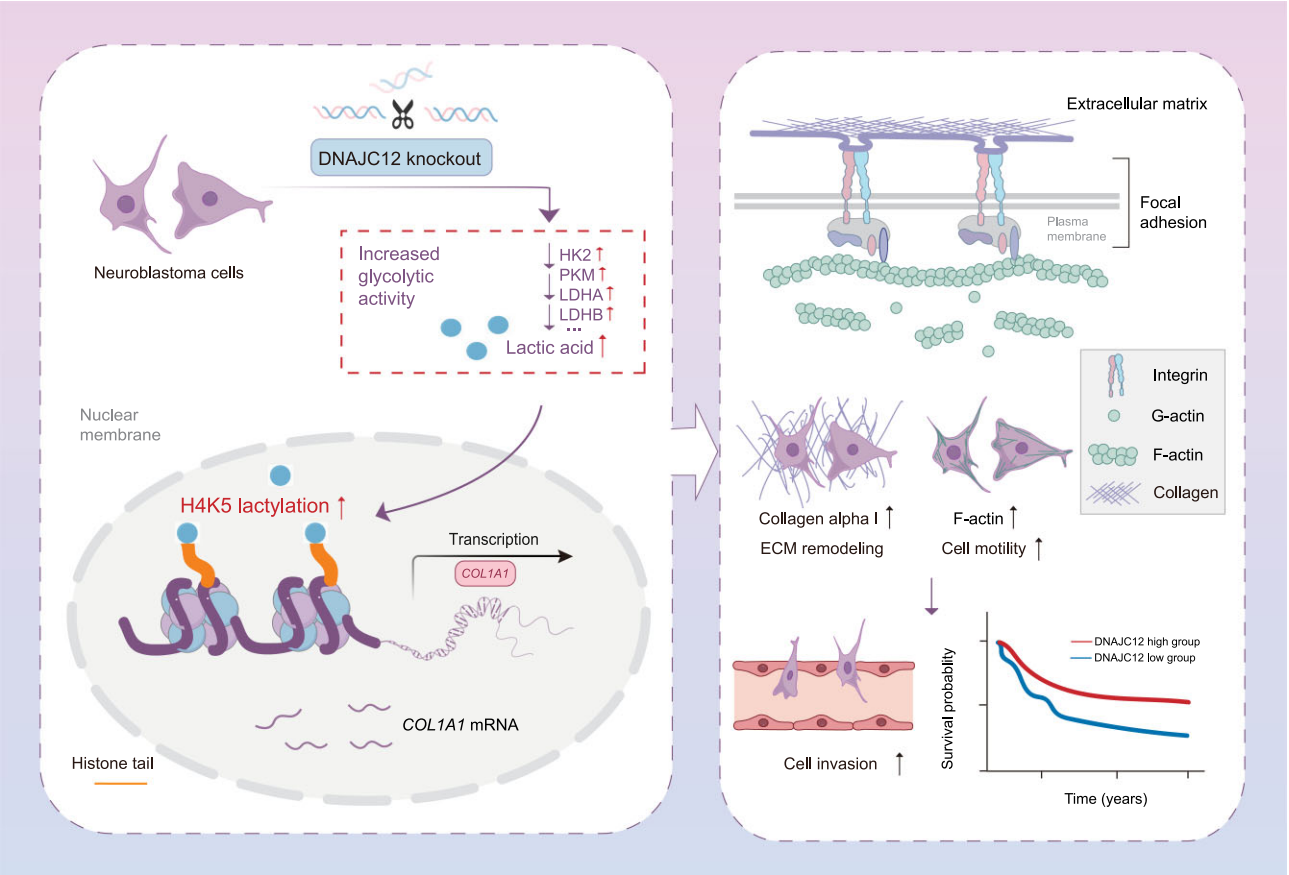

Figure 8 Schematic presentation of the DNAJC12's role in driving NB progression via metabolic and epigenetic regulation. DNAJC12 downregulation in NB cells enhances glycolysis, subsequently increasing lactate production and histone H4K5la modification. This modification upregulates *COL1A1* expression, which promotes metastatic potential by activating biomechanical force.

different cancers underscore its complex role in metabolic reprogramming, indicating that therapies targeting DNAJC12 may need to be tailored to the metabolic profile of each cancer type.

Our study identifies H4K5la as a novel prognostic marker for NB that is linked to glycolysis activation due to low DNAJC12 expression. While *MYCN* amplification is a well-known marker for poor prognosis (Durbin et al., 2022; Zhang et al., 2023), it is present in only ∼20% of NB cases (Dzieran et al., 2018) and requires complex detection methods such as sequencing or fluorescence *in situ* hybridization (Mathew et al., 2001; Yue et al., 2017), limiting its use in resource-constrained settings. Similarly, other prognostic markers, such as *ALK* mutations (Bresler et al., 2011) and *TERT* rearrangement (Huang et al., 2020), also have detection limitations. In contrast, H4K5la is widely present in NB cells and can be easily detected via IHC staining, offering a more accessible way to identify high-risk patients and tailor therapeutic strategies.

Histone modifications have emerged as important markers in cancer prognosis (Geffen et al., 2023). For example, loss of H3K27me3 due to H3K27M mutation has been identified as the causal factor of glioma (Lewis et al., 2013; Chung et al., 2020). In the context of NB, we and others also reported the dysregulation of various histone modifications related to NB progression. For example, the increased levels of H3K4me3, H3Q5ser, and H4K8la are related to NB cell proliferation and migration (Sun et al., 2015; Zhao et al., 2021; Zu et al., 2022). However, clinical application of these markers is limited. Our identification of the association of H4K5la with NB prognosis and its ability to be detected in clinical samples suggest that H4K5la could serve as a reliable biomarker for the early and accurate identification of high-risk patients.

The interactions among DNAJC12 expression, histone lactylation, and *COL1A1* gene regulation present promising therapeutic targets. *COL1A1*, which encodes type I collagen, plays a role in promoting tumor growth and invasion by supporting tumorigenesis through ECM remodeling (Tian et al., 2021; Comba et al., 2022). Targeting this pathway could provide new strategies to limit NB metastasis (Horwacik, 2022). However, our findings require validation in larger patient cohorts and preclinical models to confirm the roles of DNAJC12 and H4K5la in NB progression and their potential as therapeutic and prognostic markers.

In conclusion, our research reveals a novel pathway involving DNAJC12 downregulation and metabolic–epigenetic

reprogramming in NB progression (Figure 8). These findings pave the way for innovative diagnostic and therapeutic strategies, emphasizing the need for comprehensive approaches that integrate metabolic and epigenetic insights to better understand and manage NB.

Materials and methods

Cell lines and cell culture

The human NB cell lines SH-SY5Y and SK-N-SH, along with human embryonic kidney (HEK) 293T cells, were obtained from the Cell Bank of Type Culture Collection of the Chinese Academy of Sciences. SH-SY5Y and SK-N-SH cells were cultured in a 1:1 mixture of Eagle's minimum essential medium (EMEM; ATCC) and Ham's F12 medium (Gibco) supplemented with 10% fetal bovine serum (FBS; Nanjing Ozfan Biotechnology). HEK293T cells were cultured in Dulbecco's modified Eagle's medium (HyClone) supplemented with 10% FBS. All cell lines were maintained at 37°C in a 5% CO_2 atmosphere, and the culture medium was replaced every 3 days. Cell line authentication was performed periodically via short tandem repeat profiling, and all experiments were conducted with mycoplasma-free cells.

Pharmacological inhibitors and antibodies

The LDHA inhibitor (R)-GNE-140, the type I collagen synthesis inhibitor halofuginone, and the p300/CBP inhibitor anacardic acid were purchased from MedChemExpress and SelleckChem. The primary antibodies used included pan-Kla, H4K5la, H3K18la, H3K14la, H4K8la, H2BK16la, H3K9la, H4K16la, H4K12la (PTM-1401RM, PTM-1407RM, PTM-1427RM, PTM-1414RM, PTM-1415RM, PTM-1424RM, PTM-1419RM, PTM-1417RM, and PTM-1411RM, respectively, from PTM BIO), DNAJC12 (Proteintech, 12338-1-AP), GAPDH (Yeasen, 30203E10S), and β-actin (CWBIO, CW0096) antibodies. The horseradish peroxidase (HRP)-linked goat anti-rabbit secondary antibody was purchased from Cell Signaling Technology (7074S).

NB patients' survival analysis

Survival data for 249 NB patients (Supplementary Table S1) were obtained from the TARGET database (https://www.cancer.gov/ccg/research/genome-sequencing/target). The patients were stratified into high- and low-expression groups on the basis of median *DNAJC12* expression levels. Kaplan–Meier survival analysis was performed, and survival differences were assessed via the log-rank test.

Generation of DNAJC12 KO SH-SY5Y and SK-N-SH cells using CRISPR/Cas9

DNAJC12 knockout was performed using the CRISPR/Cas9 system. The lentiCRISPR v2 vector (Addgene plasmid #52961), which was designed via the ECRISP tool (http://www.e-crisp.org/E-CRISP/), was used to clone gene-specific single guide RNA sequences (Supplementary Table S5). The lentivirus was produced by co-transfecting HEK293T cells with psPAX2, pMD2.G, and lentiCRISPR v2-derived plasmids using Lipofectamine 3000 (Invitrogen). After 6 h, the medium was replaced with fresh EMEM/F12 containing 15% FBS, and the lentiviral particles were harvested three days later. SH-SY5Y or SK-N-SH cells were infected with lentiviral particles and selected with 3 μg/ml puromycin (Gibco) 48 h post-infection. Knockout efficiency was confirmed by qPCR and immunoblotting.

Transient transfection

PLL3.7 plasmids containing 3×FLAG-tagged DNAJC12 or 3×FLAG-tagged $SIRT2^{OE}$ and $SIRT2^{Q167A}$ were transiently transfected into DNAJC12 KO SH-SY5Y cells using Lipofectamine 3000 (Invitrogen). Briefly, 7.5 μl of Lipofectamine 3000 was incubated with 2500 ng plasmids and 5 μl of p3000 reagent in OPTI-MEM medium, after which 5×10^5 cells were added. The culture medium was replaced with fresh EMEM/F12 containing 15% FBS after 6 h. The cells were harvested 72 h post-transfection for downstream analyses.

siRNA-mediated COL1A1 knockdown

siRNA sequences targeting *COL1A1* were synthesized by GenePharma (Supplementary Table S6). SH-SY5Y cells were transfected with siRNA using Lipofectamine 3000 (Invitrogen) and harvested 48 h post-transfection for qPCR and immunoblotting to analyze *COL1A1* expression.

RNA extraction and qPCR

Total RNA was extracted using TRIzol reagent (Invitrogen) following the manufacturer's protocol. Reverse transcription was performed using a Hifair® II 1st Strand cDNA Synthesis Kit (Yeasen) with 1 μg of RNA per sample. qPCR was conducted using Hieff® qPCR SYBR Green Master Mix (Yeasen), with target mRNA levels normalized to those of *ACTB* or *GAPDH*. The sequences of the qPCR primers used are provided in Supplementary Table S7.

Protein extraction and immunoblotting

The cells were lysed in sodium dodecyl sulfate (SDS) lysis buffer and subjected to immunoblotting. Lysates were separated on 8%, 10%, or 15% SDS–polyacrylamide gels and transferred to polyvinylidene difluoride membranes (Millipore). The membranes were blocked with 5% milk or bovine serum albumin (BSA) in phosphate-buffered saline (PBS) containing 0.05% Tween 20 for 1 h at room temperature. After blocking, the membranes were incubated with the appropriate primary antibodies overnight at 4°C. Then, the membranes were washed and incubated with HRP-conjugated secondary antibodies for 1 h at room temperature. The protein bands were visualized using an enhanced chemiluminescent reagent (Millipore) and detected using a chemiluminescence imaging system.

Cell viability assays

Cell viability was assessed using the CellTiter-Glo Luminescent Cell Viability Assay (Promega) according to the manufacturer's instructions. The cells were seeded in 96-well plates at a density of 5000 cells/well and cultured for 24 h. After treatment,

50 μl of the CellTiter-Glo reagent was added to each well and incubated for 10 min, and luminescence was measured using a BioTek Synergy H1 microplate reader.

Cell proliferation assays

Cell proliferation was measured using the Cell Proliferation ELISA, BrdU (chemiluminescent) kit (Roche Diagnostics GmbH) following the manufacturer's protocol. Briefly, 1×10^4 cells were seeded in opaque 96-well plates and cultured for 48 h. The cells were incubated with BrdU labeling solution for 2 h, followed by fixation, DNA denaturation, and incubation with an anti-BrdU monoclonal antibody conjugated with peroxidase. Luminescence was detected using a substrate containing luminol and 4-iodophenol, and measurements were taken using a BioTek Synergy H1 microplate reader.

Cell invasion assays

Cell invasion assays were performed using 8-μm pore size transwell chambers (Corning) with a Matrigel matrix (0.2 mg/ml diluted with chilled serum-free medium). The cells were seeded inside the Matrigel-coated chambers at a density of 1×10^5 cells per well in medium containing 1% FBS, with 20% FBS in the medium outside the chamber. After 48 h, the cells were fixed with 4% paraformaldehyde and stained with crystal violet (Beyotime Biotechnology). Invaded cells were quantified by counting cells in five random fields per view.

Immunofluorescence staining

Immunofluorescence staining for F-actin was conducted using Alexa Fluor 488-conjugated phalloidin. The cells (2×10^5) were seeded onto 14-mm round coverslips in a 12-well plate and cultured for 24 h. The cells were then fixed with 4% paraformaldehyde for 30 min at room temperature and permeabilized and blocked with 1% BSA, 0.02% Tween 20, and 0.2% Triton X-100 in PBS. Coverslips were incubated with Phalloidin-488 (ThermoFisher Scientific) and 4′,6-diamidino-2-phenylindole (DAPI) for 1 h at room temperature in the dark. After washing, the coverslips were mounted on slides, and images were captured using a Leica Stellaris 5 confocal microscope (Leica Microsystems). The integrated density (IntDen) was measured using ImageJ software.

Metabolomics

Metabolomic analysis was performed on 1×10^6 cells, which were washed with cold PBS and resuspended by 1 ml 80% methanol. The supernatant was collected by centrifugation and subjected to liquid chromatography–MS/MS. The samples were analyzed on a Q-Exactive Plus mass spectrometer (ThermoFisher Scientific) with a Merck SeQuant ZIC-pHILIC column (2.1×150 mm, 5 μm). Metabolites were quantified by calculating the peak areas.

Lactic acid measurement

The intracellular lactic acid concentration was measured with an L-Lactic Acid (LA) Colorimetric Assay Kit (Elabscience). The cells (5×10^6) were sonicated in cold PBS, and the supernatant was incubated with enzyme solution (LDH, NAD+, and PMS) and chromogenic agent (NBT) for 10 min at 37°C. The absorbance at 530 nm was measured using a BioTek Synergy H1 microplate reader, and lactic acid concentrations were calculated on the basis of a standard curve.

Patients' samples and IHC staining

Formalin-fixed paraffin-embedding (FFPE) samples from 18 NB patients treated at Shanghai Children's Medical Center between January 2018 and December 2019 were included in this study. An additional tumor sample containing intravascular tumor emboli from a patient diagnosed in 2021 was included to investigate the importance of H4K5la in NB metastasis. All patients included in the study had been diagnosed with NB and had not received chemotherapy or radiotherapy prior to tissue collection. The study protocol was approved by the Institutional Review Board and Ethics Committee at the Shanghai Children's Medical Center (SCMCIRB-K2024004-1).

FFPE samples were sectioned into 4-μm thick slices and processed for IHC staining. The tissue sections were incubated with rabbit monoclonal antibodies targeting histone lactylation at various sites, including anti-H4K5la. Following primary antibody incubation, the sections were treated with HRP-conjugated goat anti-rabbit secondary antibodies. After staining, the slides were digitized using a Leica Aperio scanner and analyzed with Aperio ImageScope (Leica Biosystems). IHC staining intensity was evaluated and scored independently by two pediatric pathologists using a standardized scoring system: negative (score 0), weak (score 1), moderate (score 2), strong (score 3), and very strong staining (score 4).

RNA-seq and data analysis

Total RNA was extracted from wild-type and DNAJC12 KO SH-SY5Y cells using TRIzol reagent (Invitrogen) following the manufacturer's protocol. RNA purification, reverse transcription, library preparation, and sequencing were outsourced to Mingma Technologies Co., Ltd, Shanghai. Sequencing libraries were constructed using the TruSeq® Stranded Total RNA Gold Kit (Illumina), which is designed to enrich polyadenylated RNA and deplete ribosomal RNA.

RNA-seq reads were quantified using Salmon, a tool for fast and accurate transcript quantification. Differentially expressed genes between wild-type and DNAJC12 KO cells were identified using DESeq2, applying a 1.5-fold change and an adjusted *P*-value <0.05 as the threshold to determine significance. GSEA was performed to identify significantly enriched pathways and biological processes, using GSEA software version 3.0 (http://www.broadinstitute.org/gsea/).

ChIP–seq and ChIP–qPCR

ChIP–seq and ChIP–qPCR were performed following a previously described protocol (Zhao et al., 2021). Briefly, 1×10^7 cells were fixed with 1% formaldehyde, lysed in SDS lysis buffer, and sonicated. Sonicated chromatin was

immunoprecipitated overnight with anti-histone H4K5la or control IgG (Cell Signaling Technology, 66362S), with spike-in antibody and chromatin (Active Motif) added as control. Chromatin precipitates were obtained with Pierce protein A/G magnetic beads (Thermo Scientific) and eluted by protease K digestion, followed by cross-link reversal for 4 h at 65°C and DNA purification using a DNA Clean & Concentrator kit (Qiagen). The immunoprecipitated DNA was used for ChIP–seq library preparation (ANOROAD) or ChIP–qPCR. The primer sequences for the *COL1A1* gene are provided in Supplementary Table S7. For ChIP–seq data analysis, reads were aligned to the hg38 reference genome using the Burrows–Wheeler Alignment tool v0.7.17-r1188, and peaks were called using MACS2 v2.2.6 after ambiguously mapped and duplicate reads. The ChIP–seq data were visualized with Integrative Genomics Viewer v2.8.13.

Statistical analysis

All the data were collected from at least three independent experiments. The results are expressed as mean ± SEM. Differences between two groups were assessed using two-tailed unpaired Student's *t*-test. Statistical analysis was performed using GraphPad Prism9 software (GraphPad Software LLC). $P < 0.05$ was considered to indicate statistical significance.

Data availability

The raw and processed sequencing data from the RNA-seq and ChIP–seq experiments conducted in this study have been deposited in the Gene Expression Omnibus (https://www.ncbi.nlm.nih.gov/geo/) under accession numbers GSE262134 and GSE262547, respectively. Any additional data supporting the findings of this study are available from the corresponding author upon reasonable request.

Supplementary material

Supplementary material is available at *Journal of Molecular Cell Biology* online.

Acknowledgements

The authors acknowledge the contributions from all the participants.

Funding

This work was supported by grants from the Fundamental Research Funds for the Central Universities (YG2022ZD021), the Natural Science Foundation of Shanghai (22ZR1440200 and 23410760900), the Science and Technology Development Fund of Shanghai Pudong New Area (PKJ2022-Y01 and PKJ2022-Y03), and the Science and Technology Commission of Shanghai Municipality (202140143).

Conflict of interest: none declared.

Author contributions: N.S., J.M., and X.M. supervised the project and designed the experiments. Y.Y., J.W., and S.L. performed the experiments. Y.H. analyzed the clinical data. Y.P. and Y.Z. performed bioinformatics data analysis. Q.H. and J.M. participated in the IHC staining and score assessment. Y.Z. discussed the data. N.S., X.M., Y.Y., and J.W. wrote the manuscript.

References

Acun, T., Doberstein, N., Habermann, J.K., et al. (2017). HLJ1 (DNAJB4) gene is a novel biomarker candidate in breast cancer. OMICS *21*, 257–265.

Anikster, Y., Haack, T.B., Vilboux, T., et al. (2017). Biallelic mutations in DNAJC12 cause hyperphenylalaninemia, dystonia, and intellectual disability. Am. J. Hum. Genet. *100*, 257–266.

Bresler, S.C., Wood, A.C., Haglund, E.A., et al. (2011). Differential inhibitor sensitivity of anaplastic lymphoma kinase variants found in neuroblastoma. Sci. Transl. Med. *3*, 108ra114.

Chung, C., Sweha, S.R., Pratt, D., et al. (2020). Integrated metabolic and epigenomic reprograming by H3K27M mutations in diffuse intrinsic pontine gliomas. Cancer Cell *38*, 334–349.e9.

Comba, A., Faisal, S.M., Dunn, P.J., et al. (2022). Spatiotemporal analysis of glioma heterogeneity reveals COL1A1 as an actionable target to disrupt tumor progression. Nat. Commun. *13*, 3606.

Deng, I.B., Follett, J., Bu, M., et al. (2024). DNAJC12 in monoamine metabolism, neurodevelopment, and neurodegeneration. Mov. Disord. *39*, 249–258.

Durbin, A.D., Wang, T., Wimalasena, V.K., et al. (2022). EP300 selectively controls the enhancer landscape of MYCN-amplified neuroblastoma. Cancer Discov. *12*, 730–751.

Dzieran, J., Rodriguez Garcia, A., Westermark, U.K., et al. (2018). MYCN-amplified neuroblastoma maintains an aggressive and undifferentiated phenotype by deregulation of estrogen and NGF signaling. Proc. Natl Acad. Sci. USA *115*, E1229–E1238.

Finnin, M.S., Donigian, J.R., and Pavletich, N.P. (2001). Structure of the histone deacetylase SIRT2. Nat. Struct. Biol. *8*, 621–625.

Friedman, D.N., Goodman, P.J., Leisenring, W.M., et al. (2024). Impact of risk-based therapy on late morbidity and mortality in neuroblastoma survivors: a report from the childhood cancer survivor study. J. Natl Cancer Inst. *116*, 885–894.

Geffen, Y., Anand, S., Akiyama, Y., et al. (2023). Pan-cancer analysis of post-translational modifications reveals shared patterns of protein regulation. Cell *186*, 3945–3967.e26.

Gu, J., Liu, Z., Zhang, S., et al. (2020). Hsp40 proteins phase separate to chaperone the assembly and maintenance of membraneless organelles. Proc. Natl Acad. Sci. USA *117*, 31123–31133.

Horwacik, I. (2022). The extracellular matrix and neuroblastoma cell communication—a complex interplay and its therapeutic implications. Cells *11*, 3172.

Huang, L., Yu, Z., Zhang, T., et al. (2014). HSP40 interacts with pyruvate kinase M2 and regulates glycolysis and cell proliferation in tumor cells. PLoS One *9*, e92949.

Huang, M., Zeki, J., Sumarsono, N., et al. (2020). Epigenetic targeting of TERT-associated gene expression signature in human neuroblastoma with TERT overexpression. Cancer Res. *80*, 1024–1035.

Jansky, S., Sharma, A.K., Korber, V., et al. (2021). Single-cell transcriptomic analyses provide insights into the developmental origins of neuroblastoma. Nat. Genet. *53*, 683–693.

Jung-Kc, K., Himmelreich, N., Prestegard, K.S., et al. (2019). Phenylalanine hydroxylase variants interact with the co-chaperone DNAJC12. Hum. Mutat. *40*, 483–494.

Ladenstein, R., Potschger, U., Valteau-Couanet, D., et al. (2018). Interleukin 2 with anti-GD2 antibody ch14.18/CHO (dinutuximab beta) in patients with high-risk neuroblastoma (HR-NBL1/SIOPEN): a multicentre, randomised, phase 3 trial. Lancet Oncol. *19*, 1617–1629.

Lewis, P.W., Muller, M.M., Koletsky, M.S., et al. (2013). Inhibition of PRC2 activity by a gain-of-function H3 mutation found in pediatric glioblastoma. Science *340*, 857–861.

Li, Y., Li, M., Jin, F., et al. (2021). DNAJC12 promotes lung cancer growth by regulating the activation of β-catenin. Int. J. Mol. Med. *47*, 105.

Liu, Q., Liang, C., and Zhou, L. (2020). Structural and functional analysis of the Hsp70/Hsp40 chaperone system. Protein Sci. *29*, 378–390.

Mathew, P., Valentine, M.B., Bowman, L.C., et al. (2001). Detection of MYCN gene amplification in neuroblastoma by fluorescence in situ hybridization: a pediatric oncology group study. Neoplasia *3*, 105–109.

Matthay, K.K., Maris, J.M., Schleiermacher, G., et al. (2016). Neuroblastoma. Nat. Rev. Dis. Primers *2*, 16078.

Ponzoni, M., Bachetti, T., Corrias, M.V., et al. (2022). Recent advances in the developmental origin of neuroblastoma: an overview. J. Exp. Clin. Cancer Res. *41*, 92.

Qian, Y.Q., Patel, D., Hartl, F.U., et al. (1996). Nuclear magnetic resonance solution structure of the human Hsp40 (HDJ-1) J-domain. J. Mol. Biol. *260*, 224–235.

Shen, M., Cao, S., Long, X., et al. (2024). DNAJC12 causes breast cancer chemotherapy resistance by repressing doxorubicin-induced ferroptosis and apoptosis via activation of AKT. Redox. Biol. *70*, 103035.

Spencer, B., Patel, A., Cilley, R., et al. (2022). Surgical management in pediatric neuroblastoma diagnosis and treatment: a 20-year, single-center experience. World J. Pediatr. *18*, 120–125.

Sterrenberg, J.N., Blatch, G.L., and Edkins, A.L. (2011). Human DNAJ in cancer and stem cells. Cancer Lett. *312*, 129–142.

Sun, Y., Bell, J.L., Carter, D., et al. (2015). WDR5 supports an N-Myc transcriptional complex that drives a protumorigenic gene expression signature in neuroblastoma. Cancer Res. *75*, 5143–5154.

Thony, B., Ng, J., Kurian, M.A., et al. (2024). Mouse models for inherited monoamine neurotransmitter disorders. J. Inherit. Metab. Dis. *47*, 533–550.

Tian, C., Huang, Y., Clauser, K.R., et al. (2021). Suppression of pancreatic ductal adenocarcinoma growth and metastasis by fibrillar collagens produced selectively by tumor cells. Nat. Commun. *12*, 2328.

Uretmen Kagiali, Z.C., Sanal, E., Karayel, O., et al. (2019). Systems-level analysis reveals multiple modulators of epithelial–mesenchymal transition and identifies DNAJB4 and CD81 as novel metastasis inducers in breast cancer. Mol. Cell. Proteom. *18*, 1756–1771.

Verhoeven, B.M., Mei, S., Olsen, T.K., et al. (2022). The immune cell atlas of human neuroblastoma. Cell Rep. Med. *3*, 100657.

Wang, J., Huang, H., and Liu, F. (2022a). DNAJC12 activated by HNF1A enhances aerobic glycolysis and drug resistance in non-small cell lung cancer. Ann. Transl. Med. *10*, 492.

Wang, N., Wang, W., Wang, X., et al. (2022b). Histone lactylation boosts reparative gene activation post-myocardial infarction. Circ. Res. *131*, 893–908.

Wu, J., Liu, T., Rios, Z., et al. (2017). Heat shock proteins and cancer. Trends Pharmacol. Sci. *38*, 226–256.

Yu, A.L., Gilman, A.L., Ozkaynak, M.F., et al. (2021). Long-term follow-up of a phase III study of ch14.18 (dinutuximab) + cytokine immunotherapy in children with high-risk neuroblastoma: COG study ANBL0032. Clin. Cancer Res. *27*, 2179–2189.

Yu, V.Z., Wong, V.C., Dai, W., et al. (2015). Nuclear localization of DNAJB6 is associated with survival of patients with esophageal cancer and reduces AKT signaling and proliferation of cancer cells. Gastroenterology *149*, 1825–1836.e5.

Yue, Z.X., Huang, C., Gao, C., et al. (2017). MYCN amplification predicts poor prognosis based on interphase fluorescence in situ hybridization analysis of bone marrow cells in bone marrow metastases of neuroblastoma. Cancer Cell Int. *17*, 43.

Zhang, D., Tang, Z., Huang, H., et al. (2019). Metabolic regulation of gene expression by histone lactylation. Nature *574*, 575–580.

Zhang, H.F., Delaidelli, A., Javed, S., et al. (2023). A MYCN-independent mechanism mediating secretome reprogramming and metastasis in MYCN-amplified neuroblastoma. Sci. Adv. *9*, eadg6693.

Zhao, J., Chen, W., Pan, Y., et al. (2021). Structural insights into the recognition of histone H3Q5 serotonylation by WDR5. Sci. Adv. *7*, eabf4291.

Zu, H., Li, C., Dai, C., et al. (2022). SIRT2 functions as a histone delactylase and inhibits the proliferation and migration of neuroblastoma cells. Cell Discov. *8*, 54.

Received June 27, 2024. Revised December 9, 2024. Accepted December 22, 2024.